water

MDPI

Article

The Potential Use of Geophysical Methods to Identify Cavities, Sinkholes and Pathways for Water Infiltration

Yawar Hussain [1,2,3,*], Rogerio Uagoda [2], Welitom Borges [3], José Nunes [2], Omar Hamza [4], Cristobal Condori [5], Khurram Aslam [6], Jie Dou [7,8] and Martín Cárdenas-Soto [9]

1 Environmental Engineering and Earth Science Department, Clemson University, Clemson, SC 29634, USA
2 Department of Geography, University of Brasilia, Brasilia 70910-900, Brazil; rogeriouagoda@unb.br (R.U.); jgustavosn@gmail.com (J.N.)
3 Institute of Geoscience, University of Brasilia, Brasilia 70910-900, Brazil; welitom@unb.br
4 Department of Built Environment, University of Derby, Derby DE22 3AW, UK; O.Hamza@derby.ac.uk
5 Department of Geology and Geophysics, National University of San Agustín de Arequipa, Arequipa 04000, Peru; ccondoriquis@unsa.edu.pe
6 Department of Earth Sciences, University of Oregon, Eugene, OR 97403, USA; kaslam@uoregon.edu
7 Three Gorges Research Center for Geo-Hazards, Ministry of Education, China University of Geosciences, Wuhan 430074, China; douj888@gmail.com
8 Department of Civil and Environmental, Nagaoka University of Technology, Niigata 40-2188, Japan
9 Department of Geophysical Engineering, National Autonomous University of Mexico, Mexico City 04510, Mexico; martinc@unam.mx
* Correspondence: yhussai@clemson.edu or yawar.pgn@gmail.com

Received: 27 June 2020; Accepted: 6 August 2020; Published: 14 August 2020

Abstract: The use of geophysical characterization of karst systems can provide an economical and non-invasive alternative for extracting information about cavities, sinkholes, pathways for water infiltration as well as the degree of karstification of underlying carbonate rocks. In the present study, three geophysical techniques, namely, Ground Penetrating Radar (GPR), Electrical Resistivity Tomography (ERT) and Very Low Frequency Electromagnetic (VLFEM) methods were applied at three different locations in relation to fluvial karst, which is listed as an environmentally sensitive area in Rio Vermelho, Mambaí, Goiás, Brazil. In the data acquisition phase, the GPR, direct-current (DC) resistivity and VLFEM profiles were obtained at the three locations in the area. Data were analyzed using commonly adopted processing workflows. The GPR results showed a well-defined lithology of the site based on the amplitude of the signal and radar typologies. On the other hand, the inverted resistivity cross-sections showed a three-layered stratigraphy, pathways of water infiltration and the weathered structures in carbonate (Bambui group). The interpretation of VLFEM as contours of current density resulted from Fraser and Karous–Hjelt filters, indicated the presence of conductive structures (high apparent current density) that might be linked to the weathered carbonate and other conductive and resistive anomalies associated with the water-filled and dry cavities (cave), respectively. The results encourage the integrated application of geophysical techniques such as the reconnaissance for further detailed characterization of the karst areas.

Keywords: Tarimba cave; ERT; GPR; VLFEM

1. Introduction

Karst processes often result in underground natural cavities due to the erosive effect of groundwater (dissolution) on carbonate rocks [1]. These features may develop caves with time which may or may not reach the surface creating sinkholes [2]. Such karst processes can significantly impact people's lives because they may cause severe damage to properties and infrastructures including

road subsidence, building-foundation collapse, dam leakage, and groundwater contamination [3,4]. In practice, these underground cavities and other karst features must be detected before the construction of any civil structures or groundwater management schemes. Another critical aspect of these caves lies in the fact that they can provide a safe and consistent habitat for particular species. Therefore, early and accurate detection of the subsurface karst conditions can play an essential role in environmental and geohazard risk assessments.

Karst areas are the subject of a broad range of studies such as archaeological, environmental hydrogeological, geological, geotechnical and geomorphological. These studies provide incomplete information about the degree of karstification without adequate data of the internal structures of the area e.g., epikarst, infiltration zones, karst conduits, cavities, presence and type of overlying sediments and thickness. The analysis of internal structures and geometry of karst is a challenging task because of the uncertainties created by the karst heterogeneities. Though, the knowledge of internal karst structures is highly essential for the vulnerability assessment of the karst aquifers (infiltration–property distribution) because it influences the infiltration conditions and other environmental aspects. The presence and thickness of overlying sediments can cause slower and diffuse infiltration, while the presence of holes or dolines and the absence of soil covert can expedite this process [5–7]. Therefore, accurate detection of such voids is valuable.

For the subsurface identification and mapping of such karst features, the non-invasive and high-resolution geophysical techniques have appeared as an appropriate choice [8–15]. In the case of natural cavities, which are usually filled with either water, air or collapsed material, a contrast is created in physical properties in comparison to the surrounding rocks. This physical contrast can be detected with the application of geophysical techniques [16]. The onset of cavities leads to the disturbance in the surrounding rocks, which are extended away from the cavity [15].

There is a wide range of geophysical methods, for example, Ground Penetrating Radar (GPR), Electrical Resistivity Tomography (ERT) and Very Low Frequency Electromagnetic (VLFEM) methods which are considered to be appropriate techniques for the delineation of conductive and resistive structures in the subsurface [17–27]. Over the past couple of decades, the applications of GPR in the karst studies have increased and many improvements have been successfully implemented [28–33]. It has been applied for the identification as well as in delineation of cave geometries and is very important in understanding karstification and speleogenetic processes that may contain useful information required for the reconstruction of the paleogroundwater flows [24]. All of these methods are capable of providing high-resolution images of the subsurface settings and can also be used to distinguish between different types of sedimentary fillings in the cavities [15].

Karst terrains are widespread in Brazil, especially in the central and eastern regions of the country, where carbonate karst occurs and is characterized by horizontally bedded and dolomite limestone having little or no relief developed under the influence of seasonal climatic variations [34]. The caves are broadly divided into two main groups as carbonated karst and non-carbonated karst of which carbonated karst is relatively more studied, however, the study of karst in Brazil is still in the infancy stage and requires further detailed analysis [34]. The prominent karst studies in Brazil are presented in the literature [35–37].

The present study applies geophysical techniques for the site characterization of the Tarimba cave, which has not been previously conducted at this site, thereby providing potential material for future detailed field campaigns. The geophysical investigations were conducted at three different sites on the karst system aiming to show the potential of the methods to identify cavities, sinkholes or paths for water infiltration. For the data acquisition, this presents an ideal site, having limestone exposures, limited or no soil cover and vegetation, and underlying shallow caves in a semi-arid region, where the karst system is dry during most of the year. Such non-invasive site characterization is crucial in environmentally sensitive areas for the identification of cavities, sinkholes (open or filled), pathways for water infiltration and delineation of the weathered carbonate structures. The study provides a

sound basis and recommendations for future investigation to improve the characterization of the karst and the geogenic protection of its underlying groundwater environment.

2. Description and Geology of the Study Area

The study area is located at the junction of the municipality of Mambaí, Goiás, Brazil (Figure 1). The Tarimba cave (which is the target of this study) has many entries and is approximately 11 km in length and partially mapped into several conduits and halls. The Tarimba is considered one of the most important caves in the region and also one of the largest in the country in terms of horizontal projection. The climate of the region is tropical with dry and rainy seasons. In the area, there are numerous rivers such as Currente, Vermelho and Buritis. The main streams flowing in the area are Bezerra, Piracanjuba, Rizada, Chumbada and Ventura. Some watercourses penetrate into the soil becoming subterranean and later surfacing, promoting the formation of caves [38,39]. The northeastern region of the State of Goiás has several geomorphological domains. Their features are evidenced by the morphostructure climate reworked, contrasting dissected and recessed forms interposed conserved forms, which represent remnants of the oldest topography. It is drained by the Paraná and Maranhão Rivers, which forms the Tocantins River [38].

The northeast region of Goiás presents lands with stratigraphic records of the Archaean, Proterozoic, Mesozoic and Cenozoic eras, most of which are Proterozoic, which includes the following units: Ticunzal formation, sequence volcanic-sedimentary rocks of Palmeirópolis and São Domingos, Arai group, Serra Branca, Tonalito São Domingos, Paranoá group and Bambuí group. The most extensive carbonate unit is the Bambuí group, which hosts the largest number of caves in Brazil [40]. The Urucuia formation representing continental fluvial deposition, restricted to the eastern portion of the area, is attributed to the Cretaceous land of Mesozoic age. The Cenozoic is represented by the current fluvial deposits, alluvial and colluvial sandy deposits and by the detritus-lateritic cover. The previous geological studies have pointed out the presence of rocks from the Urucuia group, without having details about the individual geological formations, as fine matrix sandstone (quartzstone) deposited by the wind. This is overlain by the *Serra das Araras* formation containing sandstone having thick layers of laterite, and the reddish indicates the presence of clay and rounded clasts. Transported, deposited and redeposited by the rivers and wind. In the Bambuí group, mean formation is Lagoa do Jacaré formation with undivided units of claystone and carbonate (Figure 2). The Capacete formation is the second formation of Bambuí group, which emerged because of the erosion of *Areado* group [41].

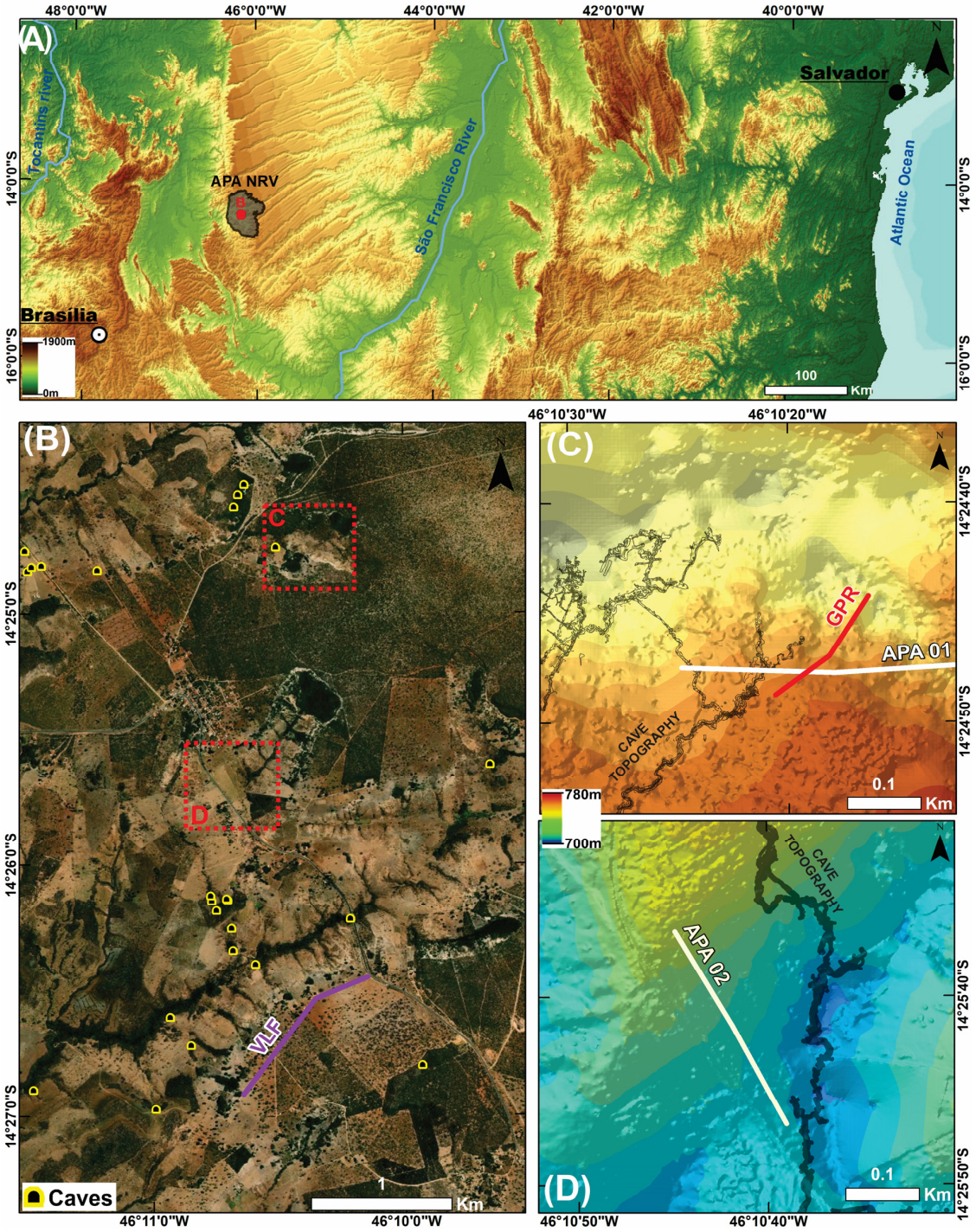

Figure 1. (**A**) Location of the environmentally sensitive area of the River Vermelho on the map of Brazil. (**B**) Locations of studied sites in proximity to the Tarimba cave and over a pavement where Very Low Frequency Electromagnetic (VLFEM) data were acquired. (**C**) Zoomed image of Site-C on high-resolution Digital Terrain Model along with a portion of Tarimba cave, the Ground Penetrating Radar (GPR) and Electrical Resistivity Tomography (ERT) survey lines. (**D**) Zoomed image of the Site-D where a resistivity (APA01) profile was taken.

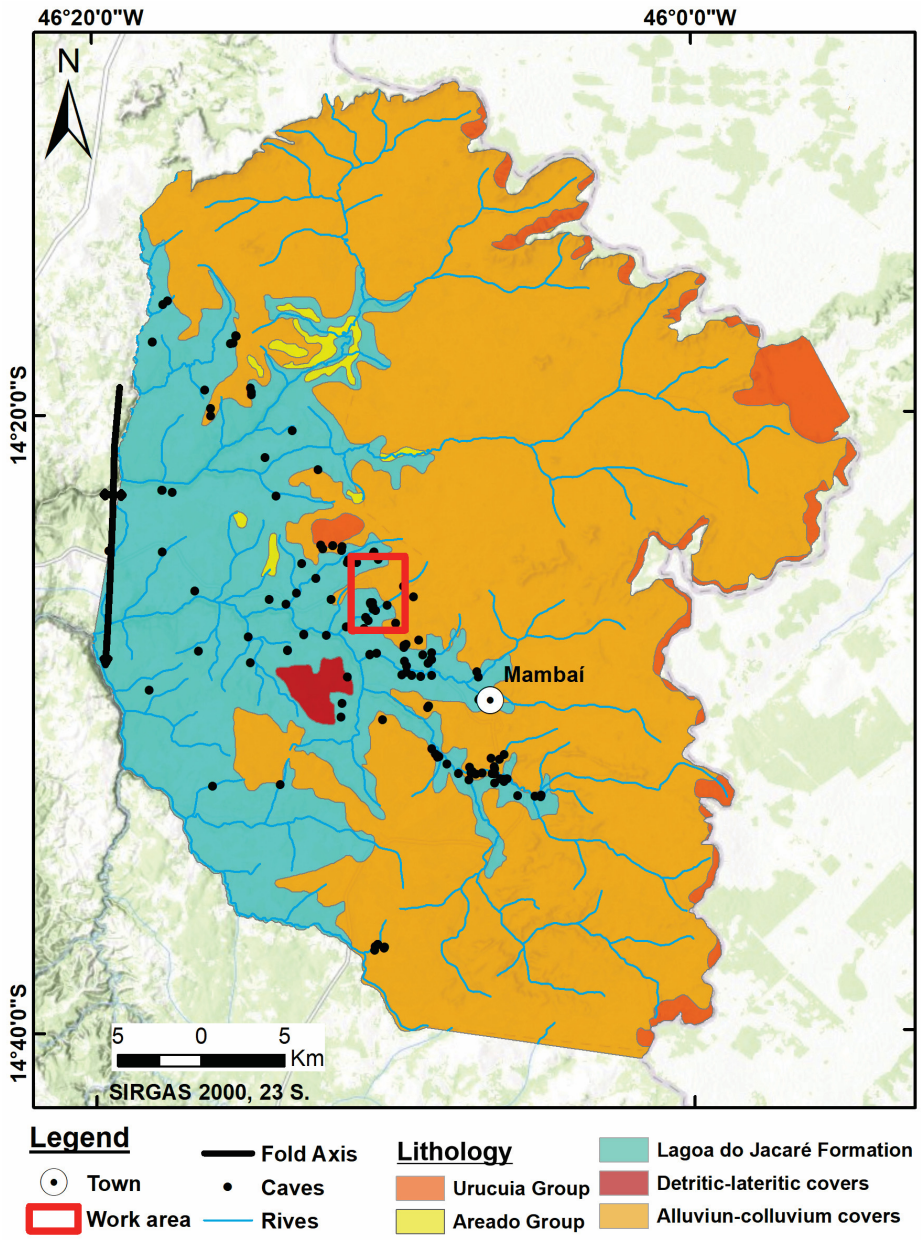

Figure 2. Geological map of the environmentally sensitive area of the River Vermelho showing different geological units, surface hydrology and the presences of mapped caves (black dots).

The general soil classification is driven from the local geology such as the Ferralsols, Arenosols and Neosols that are found in the Urucuia group. Similarly, Cambisols (being Leptosols in some places) and Acrisol (classified as Chernozem in the worksite) are found in Lagoa do Jacaré Formation. The rock stratigraphy controls the soil types. In particular, (a) Arenosols (located at the top) are connected to the presence of sandstone, and therefore the soil has more than 90% of sand in its composition, being well-drained; (b) Leptosols, are shallow soils that have around 50% of clay as developed through claystone. The presence of clay leads to the generation of a large amount of surface runoff. Finally, (c) there are irregular soils of varying depth resulted from the weathering and dissolution of the Limestone. Therefore, the composition of Chernozems depends on the presence of Limestone and the percentage of clay which may vary considerably (4–30%). This soil type is likely to be well-drained by the epikarst processes. The contact between these soils depends on the stratigraphic sequence (a possible permeable path). For example, as the *Lagoa do Jacaré* formation has an undivided

distribution of lithofacies like claystone and carbonate, at some places the sandstone (Arenosols) is in direct contact with the epikarst (Chernozem).

In most of the places, between the highly drained sandstone and the epikarst, there is a metric to a decimetric layer of claystone that may act as an impermeable layer and generates runoff. The places of contacts between the sandstone and carbonate rocks have a risk of infiltration and contamination of karst aquifers. In short, at the places where carbonate found covered by claystone, there is a high incidence of surface runoff and sediment production, which are transported reaching the karst system after entering the pathways to the caves in dolines/sinkholes. This process can cause a significant impact on the underground hydrological system. In Figure 3 different rocks units and soils types are shown.

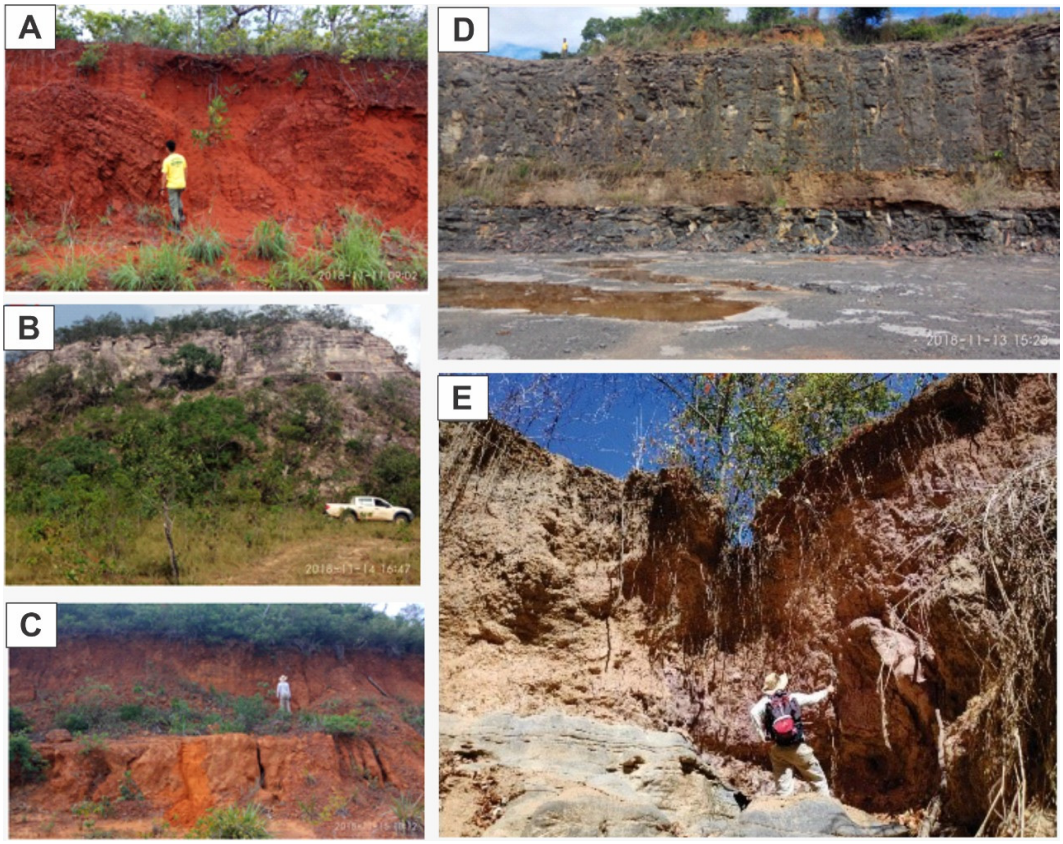

Figure 3. Photographs of different soil and rock units exposed in the area. (**A**) Ferrosols and Serra das Araras Formation. (**B**) Arenosols from Posse Formation. (**C**) Cambisols from Areal group. (**D**) Outcrop showing limestone and claystone transition. (**E**) Chernozem on top of limestone outcrop from Lagoa do Jacaré formation.

3. Materials and Methods

The study applied three geophysical techniques, including Electrical Resistivity Tomography (ERT), Ground Penetrating Radar (GPR), and Very Low Frequency Electromagnetic (VLFEM). The following sections provide a brief background about these methods and the arrangement adopted for this study.

3.1. Electrical Resistivity Tomography (ERT)

In ERT method, a potential difference is measured in response to the injection of a known amount of electrical current in the earth. Different earth materials have different resistance to the passage of current because of the variation in the degree of fractures, material types and degree of saturation. Both the injection of current and the detection of potential difference are carried out using four metal electrodes, current and potential, respectively [42]. The way in which these electrodes are

configured has a direct influence on the results, and there are two adopted ways in which electrodes are configured as (i) vertical electrical sounding (VES) and (ii) profiling. VES is applied where the target is the determination of physical property of the subsurface with depth only (1D). VES has a greater depth of penetration and spread length [43]. Profiling is used for the estimation of both vertical and lateral changes in the subsurface, as is the case with karst studies. Under these conditions, 2D and 3D images of subsurface are obtained. ERT has been applied successfully in karst studies such as their structures, soil cover and cavity geometry and more importantly the characterization of cavity sediments, the study of which is crucial for the speleology, the groundwater vulnerability and the associated geological hazards. So, the method can be used as a control for the results accuracy assessment of the other applied geophysical methods (GPR and VLFEM).

For the ERT conducted in this study, a total of 72 electrodes were used for injecting current in the subsurface as well as to measure the potential difference developed in response to these currents. The length of each profile was taken as 355 m with electrode spacing of 5 m using dipole–dipole array geometry. Two ERT profiles were taken at two different sites. The first was taken near the Tarimba cave (APA01), and the second was taken near a road (APA02, Figure 1). In the first stage, the electrical resistivity data of each line was opened in Prosycal II software in order to identify the anomalies and error in the data. Those resistivity values, which are quite high, were manually removed from the data. After the initial data editing, the RESIS2DINV of Geotomo Software [44] was used for the inversion of data where apparent resistivity values were used for the generation of a best-fit earth model. Here cell-based calculation was carried out by applying smoothness-constrained least-squares inversion method [45] where a search for an ideal subsurface resistivity best-fit model was made [46]. In this method, the subsurface is divided into rectangular blocks, each representing a single measuring point. The root means square error (RMSE) provides the discrepancy between the measured and the calculated values. Figure 4 shows an example of the observed and calculated resistivity and their interrelation of the profile APA02.

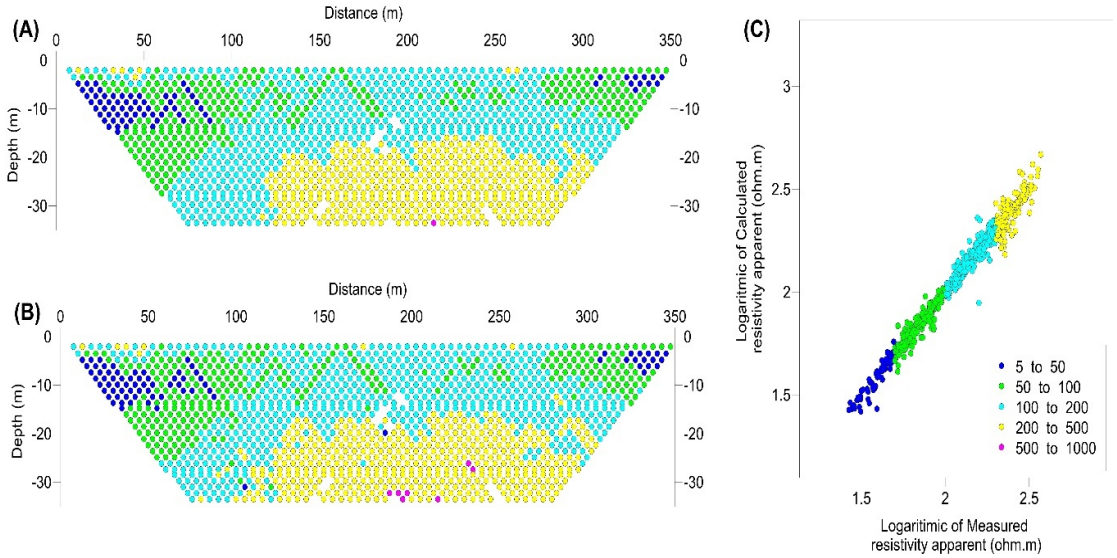

Figure 4. (**A**) Observed and (**B**) measured apparent resistivity along profile APA02. (**C**) The logarithm of the apparent vs. calculated values of APA02.

3.2. Ground Penetrating Radar (GPR)

Among different geophysical methods (including resistivity and seismic refraction) Ground Penetrating Radar (GPR) has the finest resolution—depending on the antenna used and the soil types in the area. Here, a subsurface image is obtained by passing electromagnetic waves of various frequencies through the ground. These energies are radiated from the antenna, which are either absorbed or reflected back depending on the underlying material properties such as fractures, caves, moisture and

clay contents. The energy reflected by the subsurface discontinuities is detected by a receiver, which helps in subsurface image construction. The amplitude of radar pulse is an essential factor because it can carry information about the ground. After time to depth conversion, these amplitudes help in mapping the subsurface discontinuities. The higher the contrast at the interface of these discontinuities, the higher the amplitudes are, and vice versa. A detailed description of this method and its application of cave studies is presented elsewhere [47–52]. Radar stratigraphy was used for the interpretation of reflectors. Various radar reflection typologies which may be caused by lithological and soil variations such as differences in grain compositions (e.g., presence of iron oxides), size, orientation, packing and shape of grains, changes in grain-size parameters, degree of sorting and porosity of the sediments are analyzed [53].

For this work, the GPR survey was performed using a georadar device GPR GSSI SIR 3000 (Geophysical Services Systems, Nashua, NH, USA), with 400 MHz Antenna, Control Unity and Rugged Survey Car, in order to obtain a proper resolution. One profile of 180-m length near the Tarimba was conducted, at the location shown in Figure 1C. For GPR data processing and visualization, ReflexW (Sandmeier, Inc., Karlsruche, Germany) was used, and the following necessary processing steps were employed: (i) static correction for the time zero setting; (ii) 1D Dewow filter with a pulse of 2.5-ns period was applied to remove noise induced by the electromagnetic induction of the equipment (electronic noise); (iii) removing the header which was inserted prior to the data acquisition; (iv) applying a combined gain filter (four linear and two exponential) in order to compensate abrupt changes in signal amplitude; (v) application of 2D filter for the removal of coherent noise which resulted in the areas where GPR signal attenuate quickly (the value used for the filter was 100 traces); (vi) filter application with 1D type bandpass frequency for removing random noise of high frequency, the cutting intervals of 172, 258, 688 and 828 MHz were used; (vii) collapse of diffraction with the migration of routine type diffraction stack. The values used were verified hyperbolas observed in the sandy soil at the beginning of the profile (width = 50 traces and speed = 0.1 m/s); (viii) subsequently, for the trace envelope (instantaneous amplitude) generation, the filter was applied without changing these parameters (since the same applies to the Hilbert transform data); (ix) in the end, the topography of the profile was inserted.

3.3. Very Low Frequency Electromagnetic (VLFEM)

In this semi-passive induction method, a primary field originated from distant high-power vertical transmitter (marine communications) is used. The signals from this transmitter at a frequency band of 15–30 kHz can travel a long distance and have potential geophysical implications even in areas thousands of km away from transmitters [54,55]. The horizontality of the primary field makes it an ideal choice for the investigations of vertical and dipping subsurface structures such as caves. The signals from the transmitters generate a primary field while traveling between earth surface and ionosphere. This primary field generated a secondary field which differs in the phase when coming in contact with a conductor (water-filled cave or fracture). Thus, VLF measures both primary and secondary fields and detects the conductive structures and geological contacts like altered zones, faults, and conductive caves [56,57] at an approximate depth of 30 m [58].

In the present work, VLFEM data were collected along a single profile of about 600-m length at the pavement. This site was chosen because of a lesser level of noise and easy accessibility (Figure 1B). The receiver used in this study is T-VLF unit (IRIS-Instruments, 1993), which can apply automatic filters together with the digital stacking that can improve the signal-to-noise ratio. The survey was carried out in the tilt (magnetic) mode. For the subsurface characterization using VLF data, a quantitative approach was adopted, which included examining and plotting Karous–Hjelt transform [59]. It transforms raw (unfiltered) data to current density Karous–Hjelt, the current density pseudo-sections of the VLFEM data, were produced in KHFFILT computer program [60]. The Fraser filter uses real and imaginary parts to depict a single positive, and both positive and negative peaks above a conductor, respectively. The imaginary part is used for the quality assessment of the conductor, however, in the present study,

the only real part is used for the pseudo-section of relative apparent current density variation with depth. In this way, on real data the areas of positive anomalies show zones of groundwater [61]. From the pictorial presentation of the depths of various current densities, the subsurface geological features are delineated. The pseudo-section is shown as color codes with conductivity increasing from negative to positive. Further details can be accessed in reference [27]. The positive and negative values of current values are representative of conductive and resistive bodies in the subsurface, respectively. Hence, the sub-surface features of high conductivity are identified on the VLF profile as possible fracture/weathered carbonate rocks zones and sinkholes filled with conductive materials.

4. Results and Interpretation

4.1. Electrical Resistivity Tomography (ERT)

Results of two resistivity profiles one at the entrance of the Tarimba cave, photographs of notable geological features of the area and the ERT profile taken in the area near the road, are shown in Figures 5–7, respectively. Looking at the the inverted resistivity values of APA01 (Figure 5), a three-layered stratigraphy can be seen here: a thick soil layer, then claystone and the carbonate rocks. However, the depth to the carbonate rocks is very variable, which indicates a higher degree of karstification at this location. In this way, the depressions created by the dissolved carbonate can provide a longer time for the groundwater to stay and thus had greater chances of the reaching of the contaminant to the groundwater or underlying cave. The stagnant water can also enhance the dissolution potential leading to the development of epikarst features i.e., geological hazard. The lithological contact between different rock and soil types can also influence the infiltration conditions and associated hazards.

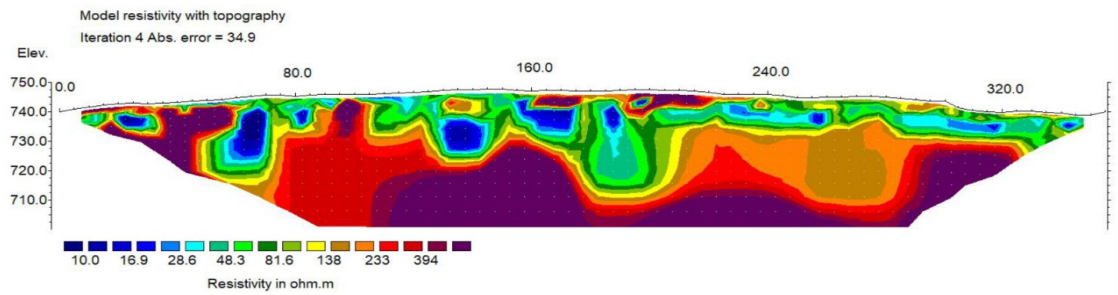

Figure 5. The modeled resistivity sections for APA01 ERT (Tarimba cave) profile. Color bar presents resistivity values in ohm.m.

Figure 6. Site photographs taken near the ERT profiles. (**A**), (**B**) of the nearby APA02 sinkholes and an erosion site, (**C**) a buried duct in the carbonate rock and (**D**) surficial opening of the Tarimba cave lies near APA01 and GPR profiles.

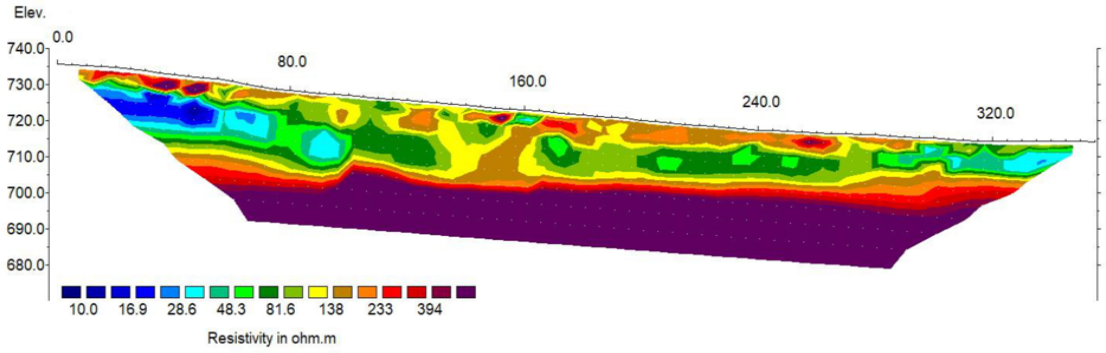

Figure 7. The modeled earth resistivity sections for APA02 ERT profile at the Site-D (road). Color bar presents resistivity values in ohm.m.

The peculiarity of the APA01 profile is, it passes through the mapped galleries and the sinkholes both open and filled on the Tarimba cave. At about 70 m from the start, it shows a low resistivity passage to the cave, that is a possible sinkhole filled with sediments having a considerable amount of moisture. Next to it is a high resistivity zone which indicates the carbonate rock. This can also be seen in the site photographs (Figure 6D). At the middle of the profile, a filled sinkhole was found, which may present geological hazards and a groundwater contamination site. This area is sensitive because of the presence of the cave openings. It is interesting to note that at the middle of the profile, a low resistivity material was found which may provide a path to water flow that dissolves the carbonate rocks. In this way, new sinkholes may emerge. These are areas which should be avoided for any future construction projects. This understructure is also crucial for the environmental and managerial planning for the cave environment of the area.

At the Site-D, the results of ERT (APA02 in Figure 7) shows a shallow resistive layer (more or less 10 m), a medium resistivity one (from 10 to 30 m maximum) and a deep resistive one. Figure 7 indicates a three-layered stratigraphy similar to the APA01 is also found here: a thick soil layer, then claystone and the carbonate rocks. In addition, ERT was successfully able to mark the presence of fracture, sinkholes and different soil types providing a different degree of geogenic protection to the cave environment. Based on the interpretation of Figure 7, the carbonate rocks were found at a depth of ~30 m and the upper layer showed clay with a high degree of moisture. This moisture content decreases with depth. Below the clay, there is an interface of claystone. It is clear from the results (Figure 7) that Tarimba cave does not pass through that site. However, there are interesting features on this site; at the beginning of the profile, a fracture-filled with sediments with varying degree of moisture and clay contents can be interpreted. There is a high probability of the presence of a sinkhole. This was also confirmed by the site visits where an active karst structure in the nearby area was found, as presented in Figure 6A,B. This edge of the profile is adjacent to the Tarimba cave passage near the ground surface, where the area is heavily used for the transportation of Limestone for the cement industry. At the middle of the profile (~160 m) a buried duct of intermediate resistivity can be seen (Figure 6C), which might be attributed to the presence of coarse-grained material. This structure may have a significant impact on karst because it can provide pathways to the precipitation for infiltration leading to the dissolution of the below karst. Therefore, their study is crucial in the risk management of heavy structures such as a road in this case. Another important aspect is the fast movement of the contaminants in the caves, that can cause possible damage to the underlying karst habitat. It can be assumed that there may be an active karst structure at the start of this profile whose geometry cannot be delineated because of the shorter length of the profile. This structure may also recreate other geological hazards in the adjoining areas. Therefore, for the safety of the nearby population and the road users, further detailed investigations are recommended.

4.2. Ground Penetrating Radar (GPR)

Using the GPR method, a profile was taken outside the cave at a location where various lithologies are present. Figure 8 shows the vertical cross-section of the subsurface of the area obtained from the reflection of electromagnetic waves. Three georadar amplitude typologies are delineated (Figure 8). Based on the field description, these typologies are linked with the different subsurface materials. The amplitudes of the electromagnetic waves are divided into three categories as high, intermediate and low. At the beginning of the profile, there found Quarts-sand Neosol (sandstone) through which the electromagnetic wave can pass easily. As a result, high amplitude reflection was observed on the 2D cross-section (Figure 8). At the middle of the profile, material absorbed the electromagnetic waves and gave rise to low amplitude wiggles. This high attenuation medium is attributed to the presence of Leptosols resulted from the in situ weathering of claystone. At the end of the profile, there are patches of Chernozem and limestone, the presence of which caused some radar wiggles of high amplitude to appear on the cross-section.

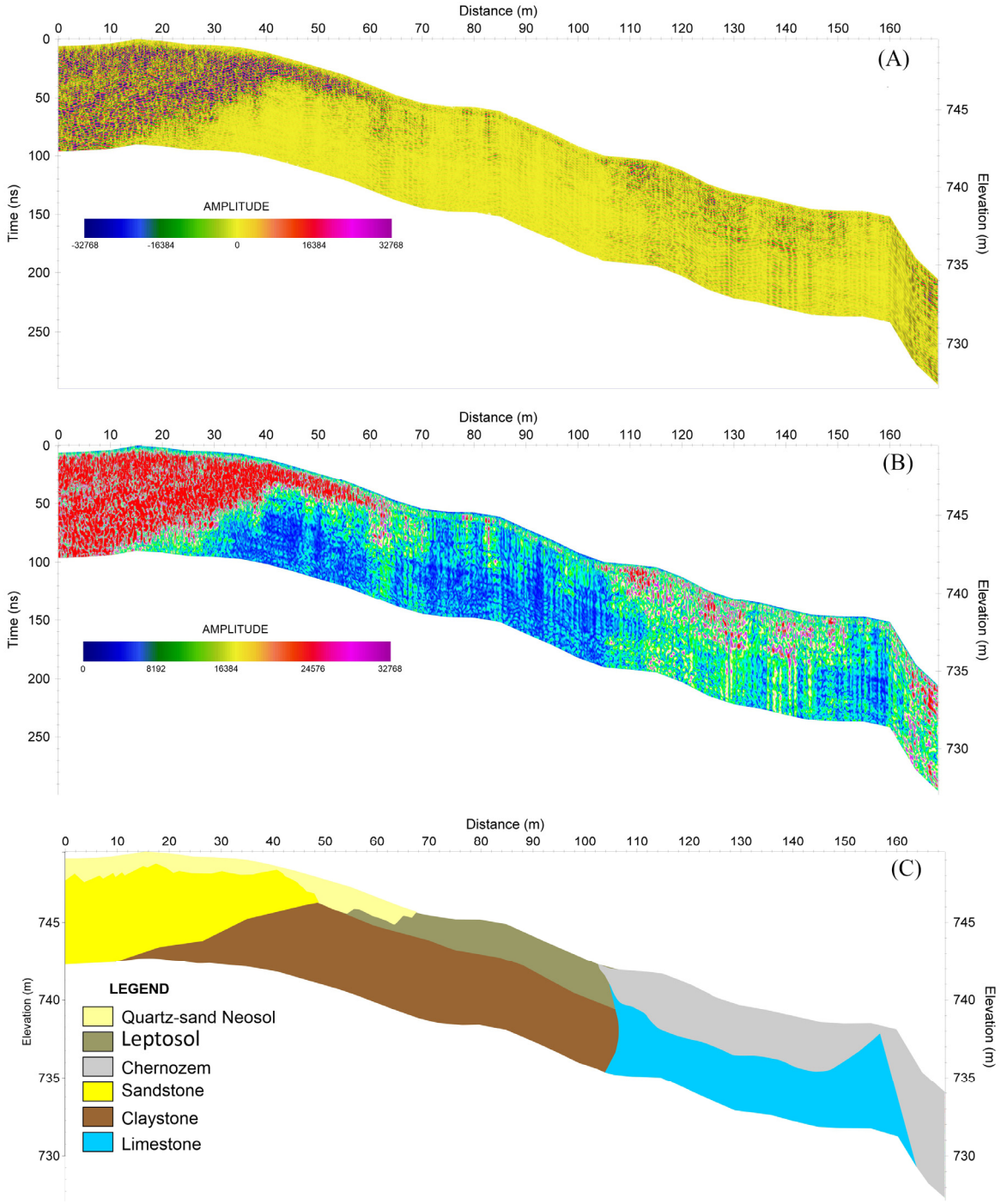

Figure 8. (**A**) GPR results, the color bar represents the values of georadar amplitude. (**B**) Instantaneous amplitude of georadar calculated after applying Hilbert transformation and (**C**) lithological cross-section obtained from GPR amplitude. Different soil types as well as a sharp contact between the carbonate of Bambui group and soil is evident. Prominent georadar typologies are focused on in Figure 9.

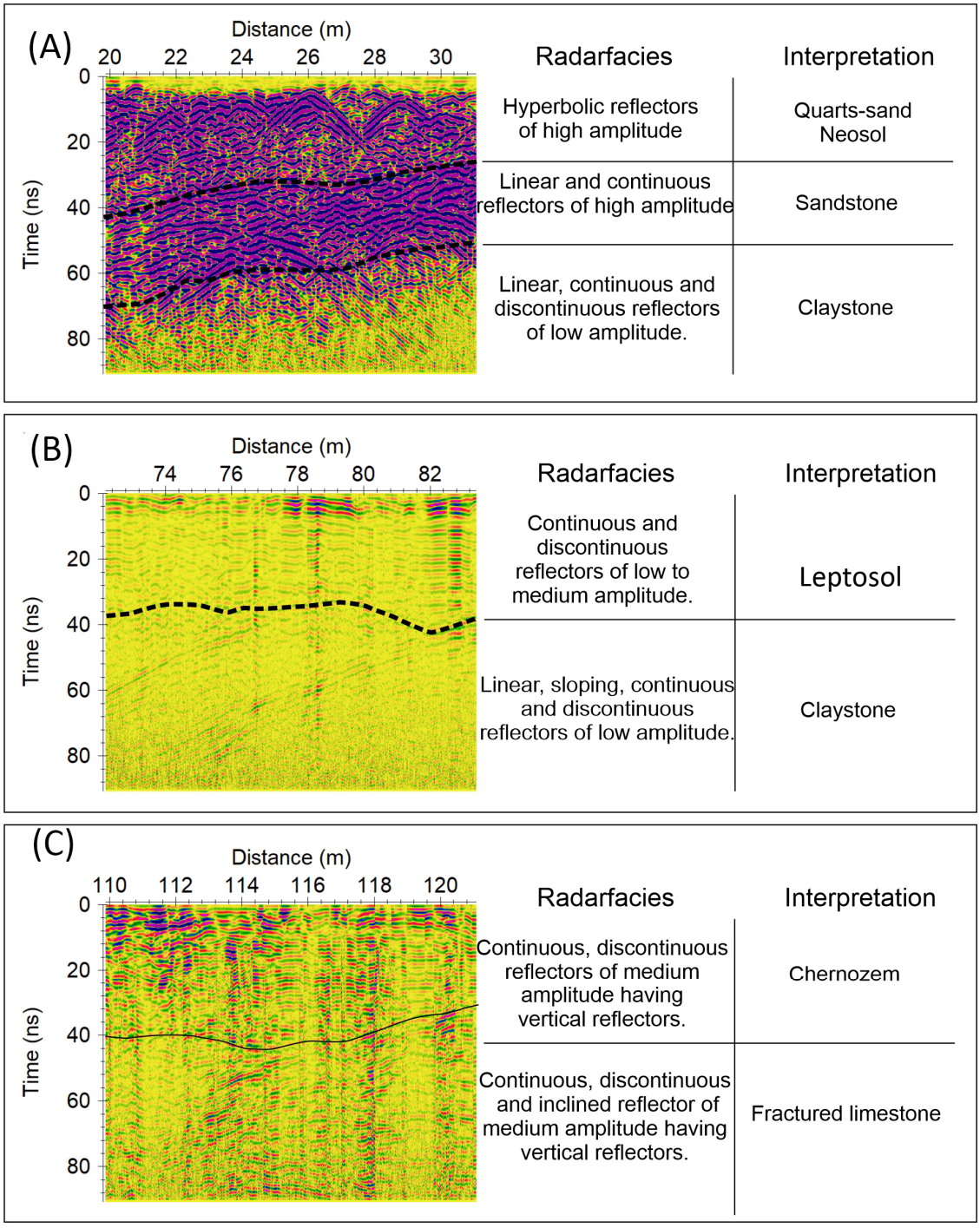

Figure 9. The prominent radar typologies. Zoomed images of different radar images along with the possible lithofacies shown in Figure 8. (**A**) High amplitude reflections associated with sandstone and Neosols, (**B**) low energy reflections may indicate the presence of conductive material possibly Leptosols and claystone and (**C**) intermediate amplitude reflections (energy) indicate the presence of Chernozem.

The various georadar typologies were also found (Figure 9) based on the amplitude and geometries of the reflectors such as continuous, discontinuous, linear and inclined. These radar typologies can be used for the delineation of different subsurface structures and soil types that can influence groundwater vulnerability. Quartzarenic neosol, are delineated as hyperbolic reflectors of high amplitude on the radargram. Below these soil types lie the sandstone as linear, contentious and high amplitude reflectors. Below sandstone lies claystone as linear, continuous and discontinuous reflectors of low

amplitude (Figure 9A). On the middle portion of the profile, there lies the Leptosol as a continuous and discontinuous reflector of low amplitude throughout the entire depth of the profile (Figure 9B). At the end of the profile, the typologies appear as contentious, discontinuous reflectors of intermediate amplitude having vertical reflections which are associated with the possible presence of Chernozem. Below, there is a zone having discontinuous inline reflectors of medium amplitude that are vertical; these are linked with the presence of weathered carbonate (Figure 9C). They are presented on the georadar images and continuous medium amplitude reflectors which can be associated as potential water flow pathways. These are essential hydrogeological features, the presence of which can increase the vulnerability of the sites. They may also be considered as the potential recharge sites for the underlying aquifer.

These different soil and rock types have their significant role in the infiltration conditions that lead to the aquifer vulnerability, generation of surface runoff and the aquifer recharge. The presence of Leptosols from claystone which has greater proportions of fine-grained material or clay proportions, low permeability can potentially inhibit the infiltration, generate the larger amount of surface runoff with sediments' load that can enter the cave. This large sediment influx in the cave can also have negative impacts on the cave habitat. These specific soil and rock types can also significantly reduce groundwater recharge. However, previous studies found higher clay content, and rich iron/aluminum oxides/hydroxides in sediments can affect the GPR depth of penetration [24]. The reverse is true for the Neosol from sandstone with greater proportions of the coarse grain material, which can increase the infiltration, thus lowering runoff and sediments' load. This soil type is also conducive for the greater depth penetration of GPR. This relation of electromagnetic wave amplitude and grain size, changes in porosity, and changes in the coefficient of reflectivity have been extensively studied [62,63].

4.3. Very Low Frequency Electromagnetic (VLFEM)

With apparent current density cross-section plots, it is possible to qualitatively discriminate between conductive and resistive structures where a high positive value corresponds to conductive subsurface structure, and low negative values are related to resistive one. Different features of varying degrees of conductivity coinciding with points already identified on the profiles (as fractures or geological features) were delineated on the section. Some of these conductive materials are linear, while others are dipping features [64]. The apparent current density cross-section of the profile VLFEM (Figure 10) revealed the presence of a significant high conductive anomaly at about 150 m from the start of the profile. Furthermore, three high current density zones at about 40 m and 320 m along the profile (Figure 10) can also be inferred as indications of the potential subsurface caves or fractured aquifer as evident from the various groundwater developments in the adjoining areas. There is a dipping conductive structure which can be a potential zone of groundwater development. It is quite interesting to note that throughout the entire length of the profile, structures of intermediate resistivity values can be seen. These indicate the possible presence of the weathered or dissolved carbonate structures, dry ducts, weathered limestone and buried dolines and caves. This may also indicate the presence of groundwater as there have already been numerous installed water pumps in the area. These structures are also crucial for the assessment of geological hazards impacting the people living nearby as well as for the cave habitat. As described in Section 4.1, such conductive structures can also increase the probability of groundwater contamination by anthropogenic contaminants. In short, VLFEM has appeared as a non-invasive reconnaissance tool for the area which guides the future details of studies and a guide for the inversion of geophysical methods such as ERT especially, in the areas where direct drilling of boreholes is not allowed.

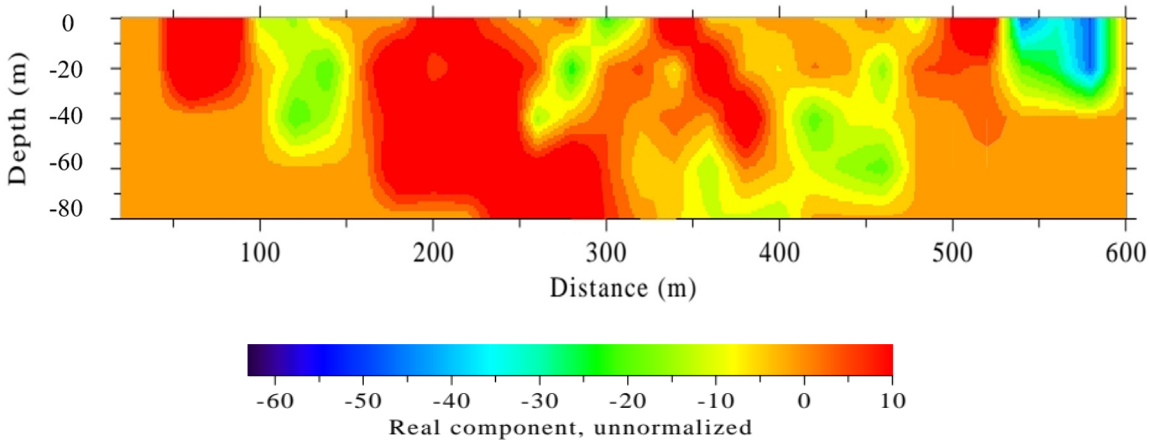

Figure 10. Karous–Hjelt current density pseudo-section showing inferred/potential conductive and resistive structures along VLFEM profile. Current density scale is arbitrary color codes with conductivity increasing from negative to positive. The high positive value constitutes the conductive sub-surface, and low negative value represents a resistive subsurface.

5. Discussion

In the case of covered karst (of Mambai), the properties of soil and the degree of karstification that are related to the development of karst features such as sinkholes, conduits and degree of weathering affect the underlying groundwater flow system. This leads to the vulnerability of fauna and flora of the caves, i.e., a threat to the cave habitat. Under these conditions, the thickness of the soil and the degree of karstification can protect the system. A high vulnerability is associated with thinner soil, coarse-grained soil, and a lesser degree of karstification.

The applied methods have their limitations and advantages in the characterization of karst areas, such as Mambaí. The comparative remarks of the methods can be made based on the data acquisition, processing as well as interpretation, spatial resolution and depth of the penetration. In terms of depth of penetration and data acquisition and processing, VLFEM should be the top choice. However, results are not so reliable because of the noise levels created by the proximity to the electrical cables, metal bard and other technical issues.

The other appropriate choice to achieve considerable high resolution at greater depths is ERT. In the present study, the ERT was able to delineate very important subsurface hydrogeological and hazardous subsurface conditions. The cavities, collapsed sinkhole, the geometries of the filled karst structures and the well-defined site stratigraphy. The georadar was better able to identify soil types, their interfaces and the pathways for water infiltration at a finer resolution as compared to other used methods.

The three geophysical techniques applied at three different locations over the karst area showed a well-defined stratigraphy. The detailed hydrogeological features were observed on the ERT profiles at greater depth. The GPR also provided results in detail; however, it was not possible to reach similar depths as achieved by ERT. The karst of the area was found covered under a clay layer that had possibly attenuated the radar energies which resulted in a relatively shallow depth of investigation. Therefore, GPR is not recommend for the investigation of caves in the areas which lie at a depth >40 m. Nevertheless, it can be used for the investigation of soil type and depth, both of which are essential input data for any vulnerability assessment model.

VLFEM results are very good here as a detailed picture of the subsurface is obtained at a greater depth. On the pseudo 2D cross-section of the current densities, the conductive and resistive anomalies are clear which may present important hydrological sub-surface features such as caves filled with water and dry caves at greater depth. These features were not delineated with ERT and GPR. Therefore, the reliability of VLFEM results is less than the other two methods, especially ERT. However,

the measurements have a poor signal-to-noise ratio on the profiles near ERT and GPR profiles. Because of that reason, the inter-comparison among these applied methods is possible.

6. Conclusions

This research demonstrated that geophysical methods have different capabilities to detect a karst system. However, it is necessary to use more than one method to obtain imaging and contribute to reducing the vulnerability of the water reservoir.

The resistivity section of ERT along the Site-D did not show the presence of a cave or groundwater. However, the inverted resistivity sections at the Site-C revealed the presence of cave and fractures, highlighting the need for further investigation for the groundwater prospecting.

Based on the GPR profiles, it was possible to distinguish between different rock units. In this way, the GPR has proved an attractive choice for the site characterization in the selected karst areas. However, because of the highly conductive soil cover, it was not possible to obtain information about the presence of caves using electromagnetic waves. Therefore, GPR is not suitable for the investigation of deeper karst structures in the covered karst area having Leptosols and claystone.

Qualitative interpretation of VLFEM profiles using different linear filtering methods such as Fraser and Karous–Hjelt showed subsurface low resistivity zones. The VLFEM profiles revealed conducting bodies associated with the presence of subsurface cavities (karst features) with a large amount of moisture. The VLFEM is an attractive choice for the reconnaissance of sensitive areas like Tarimba, where the drilling of boreholes is not permitted. Over such areas, the information derived from the VLFEM is useful for the planning of the other geophysical surveys such as ERT, GPR, and seismic-based methods. The rough information of VLFEM can be used in the inversion of these geophysical methods.

Author Contributions: Conceptualization, Y.H.; methodology, Y.H.; software, Y.H. and W.B.; validation, Y.H.; formal analysis, Y.H.; investigation, Y.H., J.N.; data curation, Y.H.; writing—original draft preparation, Y.H.; writing—review and editing, Y.H., O.H., M.C.-S., C.C., K.A., J.D.; visualization, Y.H.; supervision, R.U.; project administration, R.U.; funding acquisition, R.U. All authors have read and agreed to the published version of the manuscript.

Funding: This research was funded by TCCE 01/2018—Vale/ICMbio, PROCESS Nº: 02667.000110/2017-10 "Susceptibilidade, Hidrologia e Geomorfologia Cárstica Aplicadas à Conservação do Patrimônio Espeleológico da Área de Proteção Ambiental das Nascentes do Rio Vermelho." DOU N.99 SEÇÃO 3 de 24/05/2018.

Acknowledgments: We are thankful for the help received from the ICMBio Mambaí and PhyGeo-UnB in data acquisition. The authors gratefully thank São Paulo Speleology Union (UPE) for providing topography of the Tarimba Cave.

Conflicts of Interest: The authors declare no conflict of interest. The funders had no role in the design of the study; in the collection, analyses, or interpretation of data; in the writing of the manuscript, or in the decision to publish the results.

References

1. Abidi, A.; Demehati, A.; Banouni, H.; El Qandil, M. The Importance of Underground Cavities Detection in the Choice of Constructible Areas: Case of the Agglomeration of Fez (Morocco). *Geotech. Geol. Eng.* **2017**, *36*, 1919–1932. [CrossRef]
2. Mohamed, A.M.E.; El-Hussain, I.; Deif, A.; Araffa, S.A.S.; Mansour, K.; Al-Rawas, G. Integrated GPR, ERT and MASW for detecting near-surface caverns at Duqm area, Sultanate of Oman. *Near Surf. Geophys.* **2019**, *17*, 379–401. [CrossRef]
3. Gambetta, M.; Armadillo, E.; Carmisciano, C.; Cocchi, L.; Tontini, F.C. Determining geophysical properties of a near-surface cave through integrated microgravity vertical gradient and electrical resistivity tomography measurements. *J. Cave Karst Stud.* **2011**, *73*, 11–15. [CrossRef]
4. Youssef, A.M.; Al-Harbi, H.M.; Gutierrez, F.; Zabramwi, Y.A.; Bulkhi, A.B.; Zahrani, S.A.; Bahamil, A.M.; Zahrani, A.J.; Otaibi, Z.A.; El-Haddad, B.A. Natural and human-induced sinkhole hazards in Saudi Arabia: Distribution, investigation, causes and impacts. *Hydrogeol. J.* **2015**, *24*, 625–644. [CrossRef]

5. Daly, D.; Dassargues, A.; Drew, D.; Dunne, S.; Goldscheider, N.; Neale, S.; Popescu, I.; Zwahlen, F. Main concepts of the "European approach" to karst-groundwater-vulnerability assessment and mapping. *Hydrogeol. J.* **2002**, *10*, 340–345. [CrossRef]
6. Andreo, B.; Ravbar, N.; Vías, J.M. Source vulnerability mapping in carbonate (karst) aquifers by extension of the COP method: Application to pilot sites. *Hydrogeol. J.* **2008**, *17*, 749–758. [CrossRef]
7. Kavouri, K.; Plagnes, V.; Tremoulet, J.; Dörfliger, N.; Rejiba, F.; Marchet, P. PaPRIKa: A method for estimating karst resource and source vulnerability—Application to the Ouysse karst system (Southwest France). *Hydrogeol. J.* **2011**, *19*, 339–353. [CrossRef]
8. Smith, D.L. Application of the pole-dipole resistivity technique to the detection of solution cavities beneath highways. *Geophysics* **1986**, *51*, 833–837. [CrossRef]
9. Zhou, W.; Beck, B.; Adams, A. Effective electrode array in mapping karst hazards in electrical resistivity tomography. *Environ. Earth Sci.* **2002**, *42*, 922–928. [CrossRef]
10. Al-Tarazi, E.; Abu Rajab, J.; Al-Naqa, A.; Elwaheidi, M. Detecting leachate plumes and groundwater pollution at Ruseifa municipal landfill utilizing VLF-EM method. *J. Appl. Geophys.* **2008**, *65*, 121–131. [CrossRef]
11. Ezersky, M. Geoelectric structure of the Ein Gedi sinkhole occurrence site at the Dead Sea shore in Israel. *J. Appl. Geophys.* **2008**, *64*, 56–69. [CrossRef]
12. Krawczyk, C.M.; Polom, U.; Trabs, S.; Dahm, T. Sinkholes in the city of Hamburg—New urban shear-wave reflection seismic system enables high-resolution imaging of suberosion structures. *J. Appl. Geophys.* **2012**, *78*, 133–143. [CrossRef]
13. Martínez-Moreno, F.J.; Pedrera, A.; Ruano, P.; Galindo-Zaldivar, J.; Martos, S.; Castillo, L.G.; Úbeda, J.P.S.; Marín-Lechado, C. Combined microgravity, electrical resistivity tomography and induced polarization to detect deeply buried caves: Algaidilla cave (Southern Spain). *Eng. Geol.* **2013**, *162*, 67–78. [CrossRef]
14. Argentieri, A.; Carluccio, R.; Cecchini, F.; Chiappini, M.; Ciotoli, G.; De Ritis, R.; Di Filippo, M.; Di Nezza, M.; Marchetti, M.; Margottini, S.; et al. Early stage sinkhole formation in the Acque Albule basin of central Italy from geophysical and geochemical observations. *Eng. Geol.* **2015**, *191*, 36–47. [CrossRef]
15. Pazzi, V.; Di Filippo, M.; Di Nezza, M.; Carlà, T.; Bardi, F.; Marini, F.; Fontanelli, K.; Intrieri, E.; Fanti, R. Integrated geophysical survey in a sinkhole-prone area: Microgravity, electrical resistivity tomographies, and seismic noise measurements to delimit its extension. *Eng. Geol.* **2018**, *243*, 282–293. [CrossRef]
16. Bishop, I.; Styles, P.; Emsley, S.J.; Ferguson, N.S. The detection of cavities using the microgravity technique: Case histories from mining and karstic environments. *Geol. Soc. Lond. Eng. Geol. Spec. Publ.* **1997**, *12*, 153–166. [CrossRef]
17. Dourado, J.C.; Filho, W.M.; Braga, A.C.; Nava, N. Detecção de cavidades em arenitos utilizando gravimetria, eletrorresistividade e GPR. *Revista Brasileira de Geofísica* **2001**, *19*, 19–32. [CrossRef]
18. Sharma, S.; Baranwal, V.C. Delineation of groundwater-bearing fracture zones in a hard rock area integrating very low frequency electromagnetic and resistivity data. *J. Appl. Geophys.* **2005**, *57*, 155–166. [CrossRef]
19. Chalikakis, K.; Plagnes, V.; Guerin, R.; Valois, R.; Bosch, F.P. Contribution of geophysical methods to karst-system exploration: An overview. *Hydrogeol. J.* **2011**, *19*, 1169–1180. [CrossRef]
20. Abbas, A.M.; Khalil, M.; Massoud, U.; Santos, F.M.; Mesbah, H.A.; Lethy, A.; Soliman, M.; Ragab, E.S.A. The implementation of multi-task geophysical survey to locate Cleopatra Tomb at Tap-Osiris Magna, Borg El-Arab, Alexandria, Egypt "Phase II". *NRIAG J. Astron. Geophys.* **2012**, *1*, 1–11. [CrossRef]
21. Ozegin, K.O.; Oseghale, A.O.; Ogedegbe, E.O. Integrated geophysical investigation and characterization of aquifer structures in a complex environment. *Adv. Appl. Sci. Res.* **2012**, *3*, 475–480.
22. Putiška, R.; Kušnirák, D.; Dostál, I.; Lačný, A.; Mojzes, A.; Hók, J.; Pašteka, R.; Krajňák, M.; Bošanský, M. Integrated Geophysical and Geological Investiga-tions of Karst Structures in Komberek, Slovakia. *J. Cave Karst Stud.* **2014**, *76*, 155–163. [CrossRef]
23. Ammar, A.I.; Kruse, S. Resistivity soundings and VLF profiles for siting groundwater wells in a fractured basement aquifer in the Arabian Shield, Saudi Arabia. *J. Afr. Earth Sci.* **2016**, *116*, 56–67. [CrossRef]
24. Čeru, T.; Dolenec, M.; Gosar, A. Application of Ground Penetrating Radar Supported by Mineralogical-Geochemical Methods for Mapping Unroofed Cave Sediments. *Remote. Sens.* **2018**, *10*, 639. [CrossRef]
25. Fabregat, I.; Gutiérrez, F.; Roque, C.; Comas, X.; Zarroca, M.; Carbonel, D.; Guerrero, J.; Linares, R.; González, I.F.; Santolalla, F.G. Reconstructing the internal structure and long-term evolution of hazardous

sinkholes combining trenching, electrical resistivity imaging (ERI) and ground penetrating radar (GPR). *Geomorphology* **2017**, *285*, 287–304. [CrossRef]
26. Putiška, R.; Sabol, M.; Kušnirák, D.; Dostál, I. Geophysical Research at the Prepoštská Cave and Čertova Pec Cave Neanderthal Sites (Western Slovakia). *Archaeol. Prospect.* **2016**, *24*, 119–131. [CrossRef]
27. Jamal, N.; Singh, N. Identification of fracture zones for groundwater exploration using very low frequency electromagnetic (VLF-EM) and electrical resistivity (ER) methods in hard rock area of Sangod Block, Kota District, Rajasthan, India. *Groundw. Sustain. Dev.* **2018**, *7*, 195–203. [CrossRef]
28. Collins, M.; Cum, M.; Hänninen, P. Using ground-penetrating radar to investigate a subsurface karst landscape in north-central Florida. *Geoderma* **1994**, *61*, 1–15. [CrossRef]
29. McMechan, G.; Loucks, R.G.; Zeng, X.; Mescher, P. Ground penetrating radar imaging of a collapsed paleocave system in the Ellenburger dolomite, central Texas. *J. Appl. Geophys.* **1998**, *39*, 1–10. [CrossRef]
30. McMechan, G.A.; Loucks, R.G.; Mescher, P.; Zeng, X. Characterization of a coalesced, collapsed paleocave reservoir analog using GPR and well-core data. *Geophysics* **2002**, *67*, 1148–1158. [CrossRef]
31. Ehsani, M.R.; Daniels, J.J.; Allred, B.J. *Handbook of Agricultural Geophysics*, 1st ed.; CRC Press: Boca Raton, FL, USA, 2008; p. 432.
32. Anchuela, Ó.P.; Casas-Sainz, A.M.; Soriano, M.A.; Pocoví-Juan, A. Mapping subsurface karst features with GPR: Results and limitations. *Environ. Earth Sci.* **2008**, *58*, 391–399. [CrossRef]
33. Júnior, J.A.D.R.; De Castro, D.L.; Casas, A.; Himi, M.; Lima-Filho, F.P. ERT and GPR survey of collapsed paleocave systems at the western border of the Potiguar Basin in northeast Brazil. *Near Surf. Geophys.* **2015**, *13*, 369–381. [CrossRef]
34. Auler, A.; Farrant, A.R. A Brief introduction to karst and caves in Brazil. *Proc. Univ. Bristol Spelaeol. Soc.* **1996**, *20*, 187–200.
35. dos Santos, E.S.; Silva, R.W.; Sampaio, E.E. Analysis of the risk of karst collapse in Lapão, Bahia, Brazil. *Explor. Geophys.* **2012**, *43*, 198–212. [CrossRef]
36. De Queiroz Salles, L.; Galvão, P.; Leal, L.R.B.; Pereira, R.G.F.D.A.; Da Purificação, C.G.C.; Laureano, F.V. Evaluation of susceptibility for terrain collapse and subsidence in karst areas, municipality of Iraquara, Chapada Diamantina (BA), Brazil. *Environ. Earth Sci.* **2018**, *77*, 593. [CrossRef]
37. Garcia, G.P.B.; Grohmann, C.H. DEM-based geomorphological mapping and landforms characterization of a tropical karst environment in southeastern Brazil. *J. S. Am. Earth Sci.* **2019**, *93*, 14–22. [CrossRef]
38. Lobo, H.A.S.; Bichuette, M.; Hardt, R.; De Souza Martinelli, R.; Bruno Filho, F.G.; Gallão, J.; Calvo, E.M. *Preliminary Environmental Characterization and Conservation Proposal to Gruta da Tarimba Karst System—Goiás State, Brazil*; Brazilian Society of Speleology: São Paulo, Brazil, 2015.
39. De Souza Martinelli, R.; Calvo, E.M.; Lobo, H.A.S. Exploration and mapping of dores–Tarimba–Pasto De Vacas Cave System, (MAMBAÍ, Goiás, Brasil). In Proceedings of the ANAIS do 33° Congresso Brasileiro de Espeleologia Eldorado SP, Sociedade Brasileira de Espeleologia, São Paulo, Brazil, 15–19 July 2015.
40. Auler, A.S. Karst areas in Brazil and the potential for major caves—An overview. *Bol. Soc. Venezolana Espel* **2002**, *36*, 29–35.
41. Campos, J.E.G.; Dardenne, M.A. Estratigrafia e sedimentação da bacia sanfranciscana: Uma revisão. *Revista Brasileira de Geociências* **1997**, *27*, 269–282. [CrossRef]
42. Hussain, Y.; Hamza, O.; Cárdenas-Soto, M.; Borges, W.R.; Dou, J.; Rebolledo, J.F.; Prado, R.L. Characterization of Sobradinho landslide in fluvial valley using MASW and ERT methods. *REM Int. Eng. J.* **2020**, in press.
43. Strelec, S.; Mesec, J.; Grabar, K.; Jug, J. Implementation of in-situ and geophysical investigation methods (ERT & MASW) with the purpose to determine 2D profile of landslide. *Acta Montan. Slovaca* **2017**, *22*, 345.
44. Loke, M.H. *Tutorial: 2-D and 3-D Electrical Imaging Surveys*. Geotomo Software. 2004. Available online: https://sites.ualberta.ca/~{}unsworth/UA-classes/223/loke_course_notes.pdf (accessed on 12 August 2020).
45. Sasaki, Y. Resolution of resistivity tomography inferred from numerical simulation. *Geophys. Prospect.* **1992**, *40*, 453–463. [CrossRef]
46. Colangelo, G.; Lapenna, V.; Loperte, A.; Perrone, A.; Telesca, L. 2D electrical resistivity tomographies for investigating recent activation landslides in Basilicata Region (Southern Italy). *Ann. Geophys.* **2008**, *51*, 275–285.
47. Neto, P.X.; De Medeiros, W.E. A practical approach to correct attenuation effects in GPR data. *J. Appl. Geophys.* **2006**, *59*, 140–151. [CrossRef]

48. Dos Reis, J.A.; De Castro, D.L.; De Jesus, T.E.S.; Filho, F.P.L. Characterization of collapsed paleocave systems using GPR attributes. *J. Appl. Geophys.* **2014**, *103*, 43–56. [CrossRef]
49. Fernandes, A.L.; Medeiros, W.E.; Bezerra, F.; Oliveira, J.G.; Cazarin, C.L. GPR investigation of karst guided by comparison with outcrop and unmanned aerial vehicle imagery. *J. Appl. Geophys.* **2015**, *112*, 268–278. [CrossRef]
50. Jin-Long, L.; Hamza, O.; Davies-Vollum, K.S.; Jie-Qun, L. Repairing a shield tunnel damaged by secondary grouting. *Tunn. Undergr. Space Technol.* **2018**, *80*, 313–321. [CrossRef]
51. Conti, I.M.M.; De Castro, D.L.; Bezerra, F.; Cazarin, C.L. Porosity estimation and geometric characterization of fractured and karstified carbonate rocks using GPR data in the Salitre Formation, Brazil. *Pure Appl. Geophys.* **2018**, *176*, 1673–1689. [CrossRef]
52. Oliveira, J.G.; De Medeiros, W.E.; De Santana, F.L.; Bezerra, F.; Cazarin, C. Enhancing stratigraphic, structural and dissolution features in GPR images of carbonate karst through data processing. *Near Surf. Geophys.* **2020**, *18*, 135–148. [CrossRef]
53. Lejzerowicz, A.; Wysocka, A.; Kowalczyk, S. Application of ground penetrating radar method combined with sedimentological analyses in studies of glaciogenic sediments in central Poland. *Studia Quat.* **2018**, *35*, 103–119.
54. Sungkono; Husein, A.; Prasetyo, H.; Bahri, A.S.; Santos, F.A.M.; Santosa, B.J. The VLF-EM imaging of potential collapse on the LUSI embankment. *J. Appl. Geophys.* **2014**, *109*, 218–232. [CrossRef]
55. Sharma, S.P.; Singh, A. Advancement in 2D interpretation approach in very low frequency electromagnetic measurement. In Proceedings of the 23rd Electromagnetic Induction in the Earth Workshop, Chiang Mai, Thaila, 14–20 August 2016.
56. McNeill, J.D.; Labson, V.F. Geological mapping using VLF radio fields. In *Electromagnetic Methods in Applied Geophysics, 2 (Applications), Part B, Investigations in Geophysics*; Nabighian, M.N., Ed.; Society of Exploration Geophysicists: Tulsa, Oklahoma, 1991; pp. 521–640.
57. Guérin, R.; Tabbagh, A.; Andrieux, P. Field and/or resistivity mapping in MT-VLF and implications for data processing. *Geophysics* **1994**, *59*, 1695–1712. [CrossRef]
58. Fraser, D.C. Contouring of VLF-EM data. *Geophysics* **1969**, *34*, 958–967. [CrossRef]
59. Karous, M.; Hjelt, S.E. Linear filtering of VLF dip-angle measurements. *Geophys. Prospect.* **1983**, *31*, 782–794. [CrossRef]
60. Pirttijarvi, M. *Manual of the KHFFILT Program; Karous-Hjelt and Fraser Filtering of VLF Measurements, Version 1.1a*; University of Oulu: Oulu, Finland, 2004.
61. Ariyo, S.O.; Adeyemi, G.O.; Oyebamiji, A.O. Electromagnetic VLF survey forgroundwater development in contact terrain; a case study of Ishara-reno, south-western Nigeria. *J. Appl. Sci. Res.* **2009**, *5*, 1239–1246.
62. Guillemoteau, J.; Dujardin, J.-R.; Bano, M. Influence of grain size, shape and compaction on georadar waves: Examples of aeolian dunes. *Geophys. J. Int.* **2012**, *190*, 1455–1463. [CrossRef]
63. Akinsunmade, A.; Tomecka-Suchoń, S.; Pysz, P. Correlation between agrotechnical properties of selected soil types and corresponding GPR response. *Acta Geophys.* **2019**, *67*, 1913–1919. [CrossRef]
64. Ndatuwong, L.G.; Yadav, G.S. Identifications of fractured zones in part of hard rock area of Sonebhadra District, U.P., India using integrated surface geophysical method for groundwater exploration. *Arab. J. Geosci.* **2013**, *7*, 1781–1789. [CrossRef]